Climate Dynamics (1989) 3:191-206

Climate Dynamics

General circulation model simulation of mild nuclear winter effects

AB Pittock, K Walsh, and JS Frederiksen

CSIRO Division of Atmospheric Research, Private Bag 1, Mordialloc 3195, Australia

Abstract. The climatic effects of an elevated uniform global layer of purely absorbing smoke of absorption optical depth 0.2 have been simulated using a version of the 9-level spectral model of McAvaney et al. (1978). The model was run at rhomboidal wave number 21 with convective adjustment, prognostic precipitation and soil hydrology, but fixed zonally averaged climatological cloud and fixed sea surface temperature, for constant January and July conditions with and without smoke absorption. Results show a reduction in convective rainfall in the tropics and monsoonal regions of the order of 50%, with diurnal average soil surface coolings of several degrees C except in those locations where the reduction in soil moisture is sufficient to effectively stop evaporation at the surface. In that case, small increases in temperature may occur. Results over Australia are consistent with the zonal mean picture. Run in a diurnal cycle mode, the model shows that daily maximum temperatures are more strongly affected, with soil surface coolings of the order of 2°–3° C in summer (with some local warmings) and 4°–6° C in winter. Overnight minimum temperatures cool by only 1°–2° C in both summer and winter. Possible effects of a lowering of sea surface temperature, variations in cloud cover, neglect of scattering by smoke, and infrared absorption and emission by the smoke are discussed.

1 Introduction

Since the first suggestions that the smoke generated by mass fires in a nuclear war might lead to serious global-scale climatic effects (Crutzen and Birks 1982, Turco et al. 1983), estimates of these possible effects have been produced with progressively more sophisticated climate models. These have been reviewed by Pittock et al. (1986), Pittock (1986), Warner et al. (1987), and Turco and Golitsyn (1988).

Such estimates have tended to focus on the relatively short-term effects in the first few weeks in the Northern Hemisphere, where most of the smoke would be generated. This emphasis was due in part to a lack of confidence in estimating the lifetime of smoke particles in the perturbed atmosphere, and partly to an understandable concern about the possible severity of the short-term climatic effects in highly populated regions of the Northern Hemisphere. It is evident now, however, that while the severity of the short-term surface coolings may be somewhat less than thought earlier (Schneider and Thompson 1988; Ghan et al. 1988; Mitchell and Slingo 1988), there may be significant decreases in rainfall (Ghan et al. 1988; Schneider and Thompson 1988), and the expected lifetime of the smoke remaining in the upper atmosphere after the first few weeks may be of the order of 1 year or more (Stephens et al. 1988; Post 1986; Turco and Golitsyn 1988). Because it is of particular relevance to possible effects over Australia, and to the effects in the northern hemisphere and tropics 6–12 months after a nuclear war, we have estimated the possible climatic effects of relatively small smoke optical thicknesses such as might occur in such circumstances, distributed uniformly around the globe. Previous estimates have been made by Robock (1984) with an energy balance model, and by Covey (1987) using a general circulation model, for smoke confined to latitudes 30°–70° N.

We have used several approaches. In one we have used a coupled one-dimensional model of

Offprint requests to: AB Pittock

the atmosphere and a variable depth mixed-layer ocean (Walsh and Pittock, personal communication). In another we have applied a mesoscale model of the atmosphere coupled with a multi-layered soil model, which takes into account the variable stability of the atmospheric boundary layer and the finite heat capacity of the soil in both 1- and 2-dimensional modes (Garratt, Pittock and Walsh, personal communication). In the third, which is reported here, we have used a global general circulation model (GCM) having a variable stability boundary layer, prescribed sea surface temperatures, and finite soil heat capacity. Some preliminary results of the mesoscale and general circulation model experiments were presented by Pittock et al. (1989).

2 Smoke amounts and lifetime

Penner (1986) has reviewed the published estimates of the quantity and optical properties of the smoke that might be expected after a nuclear war. She finds a wide range of estimates of resulting smoke optical depth. If the primary stocks of petroleum are not included, the uniform absorption optical depth (AOD) over the Northern Hemisphere varies from 0.2 to 4.2. Including these stocks raises the range of AOD to 0.4–6.1. In the first case, the low estimate is equivalent to 50 million tonnes of smoke with the optical properties assumed by NAS (1985), i. e., with a specific absorption of $2\ m^2g^{-1}$; while the AOD of 6.1 is equivalent to about 750 million tonnes of smoke.

These values assume that coagulation of smoke leads to a decrease in AOD, but there is strong observational evidence that the primary sub-micron spherules of soot agglomerate into sparse random clusters or chains rather than into solid spheres, unless they have gone through an intermediate water droplet stage or are oily. Berry and Percival (1986) have used fractal theory to show that the scattering and absorption cross-sections of such clusters of particles increase in proportion to the number of primary spherules. Clearly then, the Mie theory is not applicable to soot particles, which would be the most effective absorptive components of any smoke cloud. It is thus probable that the specific absorptivity of smoke clouds does not increase rapidly with coagulation. Thus, the smoke cloud AOD may remain high for a longer period than previously anticipated.

Under these circumstances the AODs range from minimum estimates of 0.4 without petroleum stocks, or 1.0 including these stocks, to much higher values. Penner's estimated extinction optical depths are greater again, by about a factor of two. These include the effect of scattering, which is relatively unimportant in terms of the solar radiation reaching the surface since most scattering is in the forward direction, except at large optical depths when scattering may significantly increase the absorption path length. Except in the experiments with the one-dimensional coupled ocean–atmosphere model (Walsh and Pittock, personal communication), we have ignored scattering by the smoke. This must lead to some underestimation of the surface cooling effects for small AOD, as shown in the one-dimensional results.

More recent data (Turco and Golitsyn 1988) suggest that typical smoke absorptivity values lie in the range of 5–9 m^2g^{-1} and are almost independent of particle size, but that the total amount of smoke likely to be released by a major nuclear war is in the range of 27–290 million tonnes. These changes relative to the values used by Penner (1986) tend to compensate, so that estimated AODs remain much as assumed in the SCOPE (Pittock et al. 1986) and NAS (1985) studies.

Further refinements in estimates of smoke absorption are dependent on more representative surveys of fuel densities in likely target areas, a better understanding of the combustion processes in mass fires, and a better understanding of the prompt removal mechanisms in fire plumes. The last is related to the hygroscopic properties and coagulation rates of smoke, and the dynamics of fire plumes of varying intensities under representative meteorological conditions. As most smoke in a nuclear war will come from urban fires fed by a complex mixture of fuels, information from experimental forest fires or oil pool fires may be of limited value.

Malone et al. (1986) demonstrated the importance of lofting of smoke in quickly separating it from the region of fast washout due to precipitation. For a war in July they showed that lofting rendered the initial height of injection of the smoke almost irrelevant and that some 40% or so of smoke remained after 40 days, beyond which it would have $1/e$ residence time (dominated by that in the Northern Hemisphere) of 5 or 6 months. In the January case, in which much less lofting occurs, only some 5%–15% of the initial smoke would remain after 40 days, depending on the height of injection; and the $1/e$ residence time after 40 days would range from only 2 weeks for low injection heights to about 1.5 months for a higher initial injection profile.

More recently, Malone and coworkers have run their model for more than 40 days and find AODs in the range 0.3 to more than 1.0 persisting in the Northern Hemisphere, and 0.1–0.3 in the Southern Hemisphere after several months (R. Malone, personal communication). Most of this smoke is contained in the modified stratosphere at altitudes between 10 and 20 km where the only removal mechanisms are expected to be gravitational settling, chemical destruction, or exchange of air with the troposphere.

Gravitational settling may be expected to be very slow, especially as the coagulation of smoke into fluffy particles or long chains is not likely to increase their fall velocity appreciably. Preliminary results of laboratory measurements of the oxidation of smoke particles by ozone (de Haas 1986) suggested a half-life in the stratosphere of the order of several weeks to several months. More recent studies by Stephens et al. (1988) give a chemical half-life for soot, at temperatures expected in the lower stratosphere, of the order of 1 year or more. Apart from gravitational settling of larger particles, the main sink of volcanic particles in the stratosphere is thought to be passage of air into the troposphere. This occurs mainly in the vicinity of the jet streams and at the winter pole. A recent estimate by Post (1986) suggests a stratospheric residence time of order 200 days.

Such long lifetimes for smoke in the stratosphere suggest that, depending on the assumed absorptivity of the smoke, for an initial injection of some 50–150 million tonnes of smoke into the lower atmosphere, smoke AODs of the order 0.1–0.3 could remain in the Northern Hemisphere stratosphere up to a full year after a war in the northern spring or summer, and of the order 0.1–0.2 in the Southern Hemisphere during the first and possibly even the second post-war southern summer.

3 Basis of the model simulations

The model used is a version of that developed by McAvaney et al. (1978), with nine levels in the atmosphere, three sub-soil levels, a stability-dependent Monin-Obukhov boundary-layer scheme, convective adjustment, three layers of zonally averaged climatological cloud, and prognostic precipitation and soil hydrology. It is a spectral model, and was run at rhomboidal wave number 21, which is roughly equivalent to a grid-point model with a horizontal resolution of about 450 km. It was run for constant January and July conditions in a diurnally averaged mode from real (observed) initial conditions for 95 days to reach equilibrium. It was then run for 105 days of control conditions and, from the same model initial conditions at day 95, for 105 days of perturbed conditions (i.e. with smoke). Further runs of 100 days with a diurnal cycle were made from day 200 in both the control and perturbed cases. Fixed climatological average sea surface temperatures were used.

For simplicity we have performed our GCM calculations assuming a uniform global layer of smoke having an AOD of 0.2, situated above the upper boundary of the model. We have neglected the additional downwards infrared heating at the surface due to the smoke layer, which would warm considerably due to its absorption of solar radiation in the visible. In fact, 50% of the solar energy absorbed in the visible by the smoke would be emitted as downward infrared, but only a fraction of this (of the order of one third) would reach the surface. Thus, the additional downward infrared from the smoke would have only a minor moderating effect on the surface cooling, which is dominated by the loss of incoming visible radiation due to the smoke absorption. The effect of smoke infrared emission has been investigated in more detail using the mesoscale model (Garratt, Pittock and Walsh, personal communication), where it is shown that the overnight minimum surface temperature is moderated by the incoming long-wave flux from the smoke more than is the daytime maximum.

Re-radiation downwards by the smoke layer of outgoing infrared radiation from the surface which has been absorbed by the smoke can be neglected for low AOD, since the infrared absorptivity of the smoke is low compared to its absorptivity in the visible (Turco et al. 1983; Ramaswamy and Kiehl 1985).

4 Results from GCM simulations

4.1 Diurnally averaged mode

Figure 1 shows the zonally averaged soil surface temperature differences, perturbed minus control, for the first 10 days after smoke was introduced in July and January, respectively. In both seasons these show surface coolings of 2°–4° C at all latitudes with substantial land surfaces, with the exception of the regions affected by the polar night. Similar plots for individual days show variations about these mean coolings of order ±2° C at latitudes with large areas of land, and larger devia-

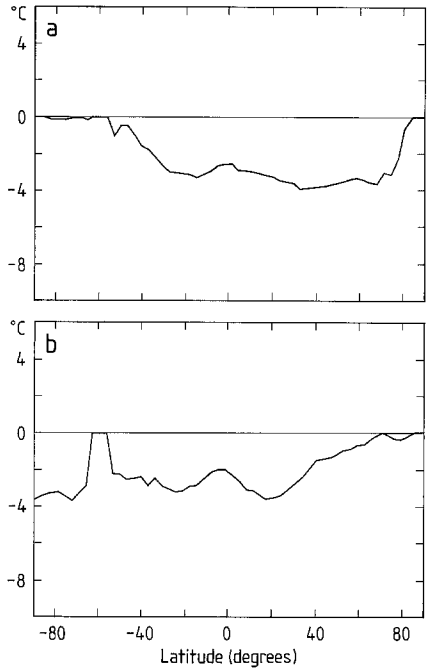

Fig. 1a, b. Zonally averaged diurnal mean soil surface temperature differences, perturbed minus control, for the first 10 days after uniform smoke of AOD = 0.2 was introduced in **a** July and **b** January

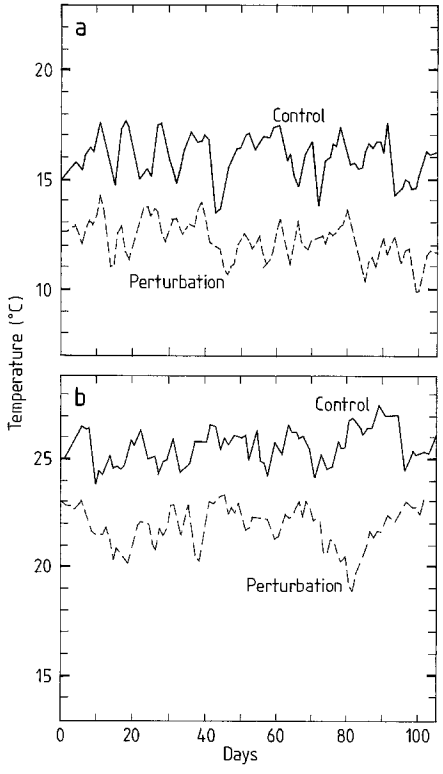

Fig. 2a, b. Time series of control *(full lines)* and perturbed *(dashed lines)* diurnal mean soil surface temperatures for **a** July and **b** January, zonally averaged at 27° S

tions where the fraction of land is small and in the high northern latitudes in winter, where large synoptic disturbances during the polar night produce large day-to-day fluctuations in both control and perturbed surface temperatures.

Figure 2 shows time series of both control and perturbed soil surface temperatures for July and January zonally averaged at 27° S, where there is a large fraction of land area. The zonally averaged cooling of order 2° C on the first day with smoke was initially rather surprising, but when data were plotted 60 times a day for the first 48 h it became evident that half the cooling occurs in the first few hours. This is reasonable, considering that the model is being run in a diurnally averaged mode, and that dry soil surfaces are observed to cool by the order of 10°–20° C under clear sky conditions during the normal diurnal cycle. Similar cooling rates were observed in mesoscale model simulations made by Garratt, Pittock and Walsh (personal communication).

At individual grid points over land, control and perturbed cases both show much larger variability due to synoptic weather events. Figure 3 is typical and shows soil surface and lowest model level (approximately 75 m) air temperatures, for January at a point in northeastern New South Wales (30° S, 152° E). Usually, but not always, the perturbed temperatures are less than in the con-

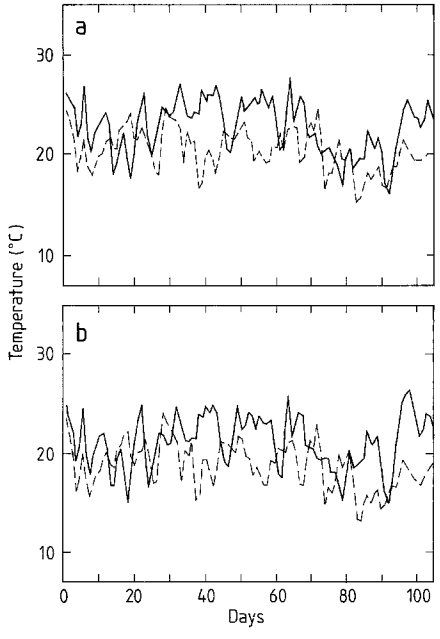

Fig. 3a, b. Time series of control *(full lines)* and perturbed *(dashed lines)* diurnal mean **a** soil surface, and **b** lowest model level (approximately 75 m) air temperatures at a grid point in northeastern New South Wales (30° S, 152° E) for January

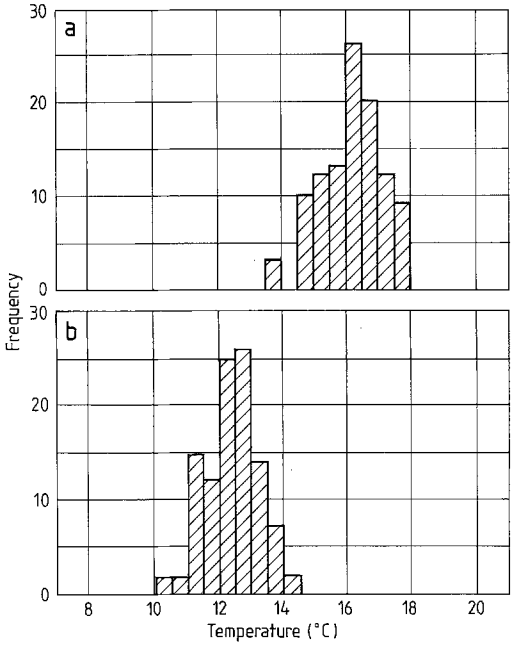

Fig. 4a, b. Frequency distributions of the 105 daily mean soil surface temperatures averaged around 27° S in July for **a** control and **b** the perturbed (smoke AOD = 0.2) simulations

trol. The time variations in the relative coolings may be partly explained, especially late in the runs when the synoptic patterns have had time to diverge somewhat, by differences in the synoptic patterns. However, much of the non-uniformity is due to differences in soil moisture which develop between control and perturbed runs due to

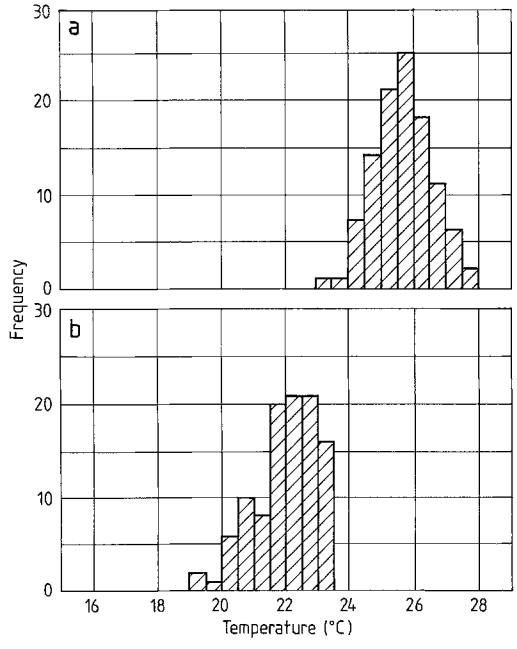

Fig. 5a, b. Same as Fig. 4 but for January

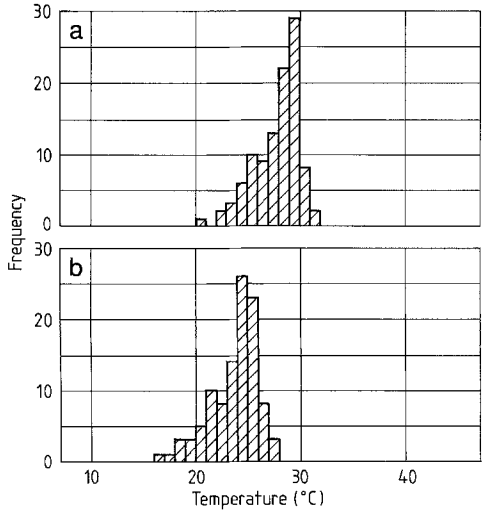

Fig. 6a, b. Frequency distributions of the 105 daily mean soil surface temperatures at a grid point in central Australia (24° S, 135° E) in January for **a** the control and **b** the perturbed simulations

changes in rainfall (see below). Note that coolings at the lowest level in the atmosphere are not, in general, much smaller than at the soil surface in the diurnally averaged runs.

Frequency distributions of the 105 daily soil surface temperatures averaged around latitude 27° S in July are shown in Fig. 4 for (a) the control, and (b) the perturbed runs. Note the cooling of more than 3° C on average, and that the distributions are single-peaked and show very little overlap. The situation is similar in January (Fig. 5), although the shape of the distribution seems to change appreciably between the control and perturbed cases. Frequency distributions for a single grid point, such as that shown in Fig. 6 for central Australia (24° S, 135° E) in January, show a larger spread of values. In this case, the average cooling is slightly larger than the zonal mean; but now the frequency distributions for the control and perturbed simulations show considerable overlap.

Zonally averaged mean precipitation rates over land are shown in Fig. 7 for July and January. Both show the control and perturbed runs for 30-day means, these being for days 71–100 in the July case and days 31–60 in the January case. These are typical results, with more variability evident in 10-day means. In both July and January there are striking reductions in precipitation rates in the Inter-Tropical Convergence Zone (ITCZ) and in the summer monsoon rainfall zones up to about 30° S (January) and 30° N (July). These reductions occur consistently in successive 10-day means, while variations outside

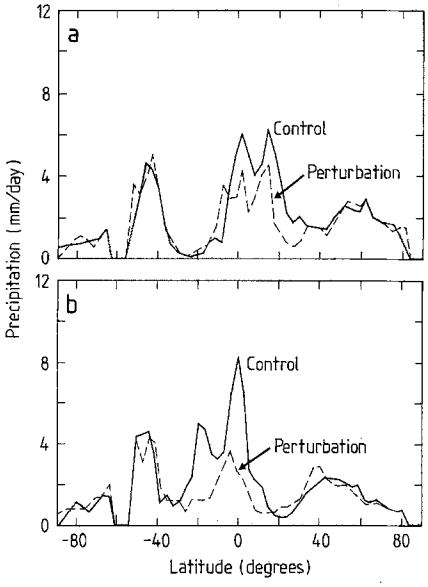

Fig. 7a, b. Zonally averaged 30-day mean precipitation rates (mm/day) over land for **a** July days 71–100 and **b** January days 31–60. Control simulations are indicated by the *full lines* and perturbed simulations (globally uniform smoke AOD = 0.2) by the *dashed lines*

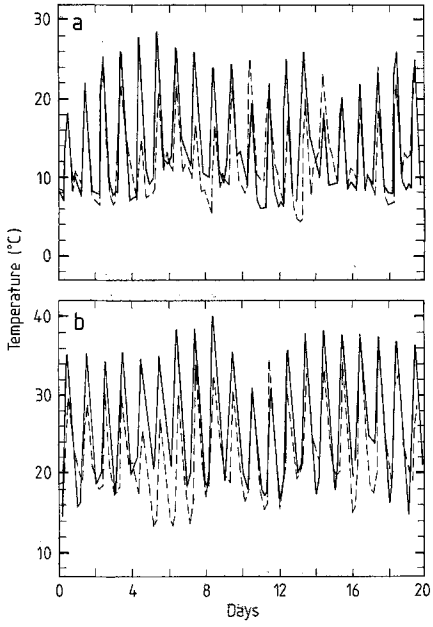

Fig. 8a, b. Time series of soil surface temperatures for the first 20 days of the diurnal mode simulations for a grid point in central Australia (24° S, 135° E) in **a** July and **b** January. Control simulations are represented by *full lines* and perturbed (smoke AOD = 0.2) by *dashed lines*

these zones are not consistent and tend to average out in longer time averages. It is striking that no significant reduction in precipitation appears in middle and high latitudes in the summer hemisphere, nor in the winter hemisphere polewards of about 15 degrees latitude. Thus, rainfall decreases of the order of 50% occur in areas of convective or monsoon rains, but not in areas where precipitation is due to extra-tropical synoptic disturbances.

4.2 Diurnal cycle mode

Time series of soil surface temperatures plotted every 4 h for the first 20 days of the diurnal runs are shown in Figs. 8a and 8b for a grid point in central Australia (24° S, 135° E) in July and January, respectively. This is a generally arid region, and the control runs (full lines) in both seasons show a mean amplitude of the diurnal cycle of around 15°–20° C. This is somewhat less than the probable actual diurnal variation in soil surface temperature, but comparable with observed screen air temperature variations (Clarke and Brook 1979). The perturbed runs (dashed lines) show a generally smaller daily cycle, with greater cooling in the daily maximum than in the overnight minimum. There are occasional days in which a relative warming occurs; these are generally days of relatively low control temperatures, indicating moist soil in the control run. Higher temperatures in the perturbed runs on these days are due to drier soil and reduced heat loss by

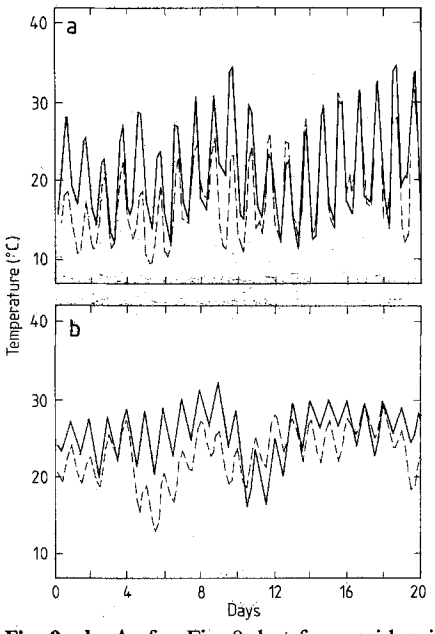

Fig. 9a, b. As for Fig. 8, but for a grid point in northeastern New South Wales (30° S, 152° E) in January for **a** soil surface temperature, and **b** lowest model level (75 m) air temperature

evaporation. This will be demonstrated more conclusively below when we examine the time series of temperature and soil moisture over the full 100 days of the diurnal runs.

Figure 9a shows similar January plots for a grid point in northeastern New South Wales (30° S, 152° E), which on the resolution of the model can be interpreted as a coastal point and far less arid than central Australia. Note the generally smaller amplitude of the daily temperature cycle in the control case compared to central Australia, but that coolings in the perturbed case are of similar magnitude to those in central Australia. Fig. 9b is the same as Fig. 9a, but for the lowest air level (approximately 75 m). Note the much smaller diurnal cycle in both control and perturbed cases, and the somewhat smaller coolings compared to those at the soil surface.

The 20-day mean diurnal cycles for the control and perturbed cases for January in central Australia are shown in Fig. 10. Note the much greater relative coolings during daylight than at night, and the effectively later onset of warming in the morning and earlier cooling to night-time conditions in the late afternoon. This is due to the greatly increased effective absorption of sunlight for large zenith angles. As noted by Pittock et al. (1986), the effective hours of daylight are appreciably reduced, and this is reflected in terms of reduced surface heating and reduced fluxes of both sensible and latent heat from the surface as shown by Garratt, Pittock and Walsh (personal communication).

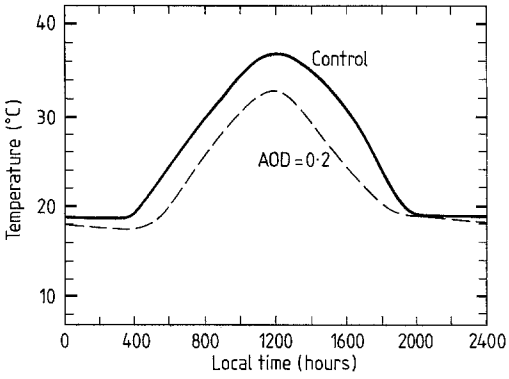

Fig. 10. The 20-day mean diurnal cycle of soil surface temperatures at a grid point in central Australia (24° S, 135° E) in January. *Full line* is the control simulation and *dashed line* that for smoke AOD = 0.2

Figure 11a shows a map of the change in daily average temperature over Australia during January between the control and perturbed cases, with the model in the diurnal cycle mode. This should be compared with Fig. 1b, which shows zonal average coolings with the model in the diurnally averaged mode. Note in Fig. 11a average coolings of the order of 2° C over much of west-

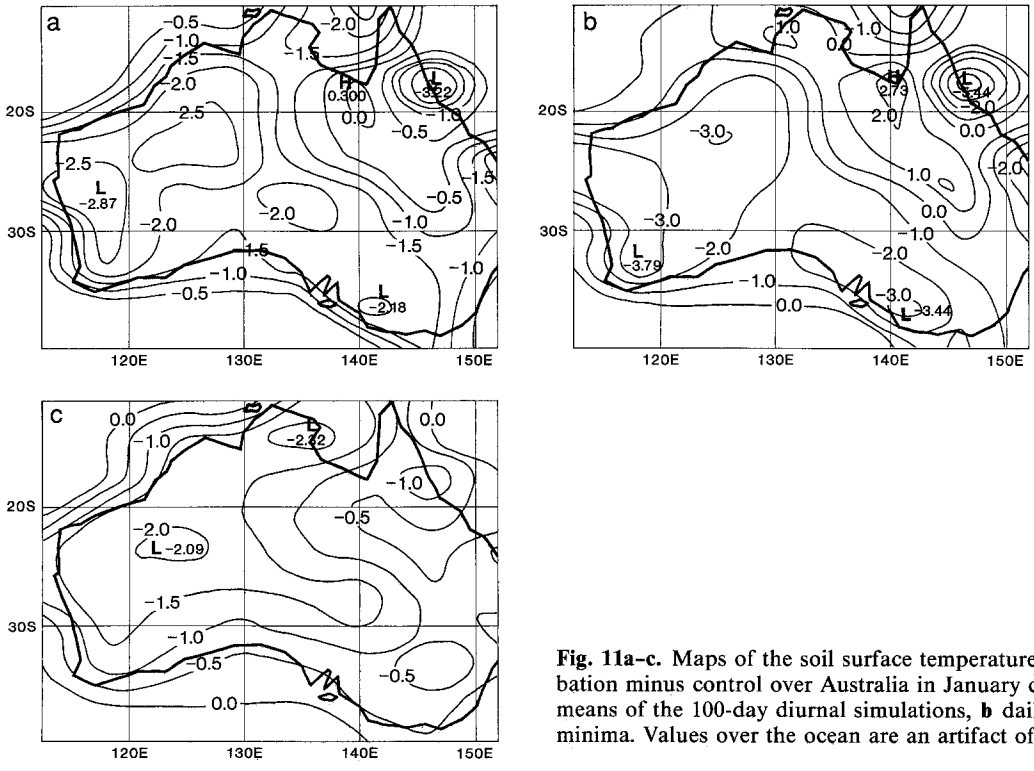

Fig. 11a–c. Maps of the soil surface temperature differences (° C) perturbation minus control over Australia in January conditions for **a** daily means of the 100-day diurnal simulations, **b** daily maxima and **c** daily minima. Values over the ocean are an artifact of the contouring program

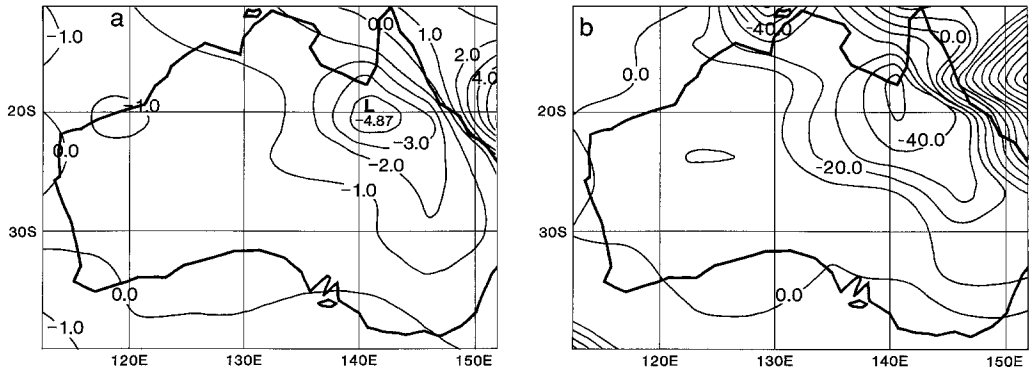

Fig. 12a, b. Maps of **a** rainfall differences (mm/day) and **b** soil moisture differences (mm, where capacity = 150 mm), for perturbation minus control over Australia in January conditions, from the diurnal mode simulations

ern and southern Australia, but coolings of less than 1° C in inland northeastern Australia. This pattern is accentuated in the map of the change in daily maximum soil surface temperature, shown in Fig. 11b. Here we see warmings of 1° or 2° C in the inland northeast, but coolings of 2°–3° C in the south and west. Falls in the overnight minimum temperatures (shown in Fig. 11c) show less variation, being in the range of 0°–2° C.

The temperature changes are largely explicable in terms of the reduction in rainfall in January, shown in Fig. 12a. Reductions in excess of 3 mm/day (80%) occur in the inland northeast, but of less than 1 mm/day (40%) in the northwest, south, and along the east coast. Indeed, rainfall does not decrease at all in the far south and along the northeast coast. The reduced rainfall, especially in the inland northeast, leads to drier soil as shown in Fig. 12b. Soil moisture changes along the south and east coasts are generally small.

In July the situation is different, with falls in the daily mean temperature in the range 3°–4° C over most of northern and central Australia (Fig. 13a). Daily maximum temperatures fall by 3°–6° C over nearly all of the country, with the smallest coolings — which are still in excess of 2° C —

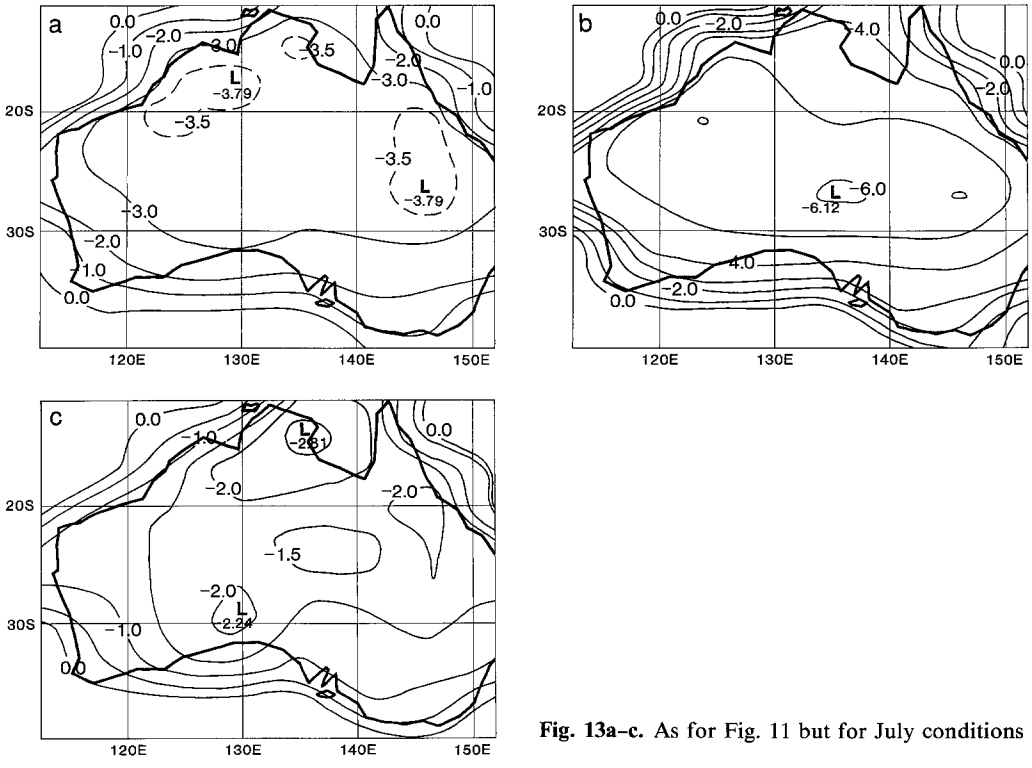

Fig. 13a–c. As for Fig. 11 but for July conditions

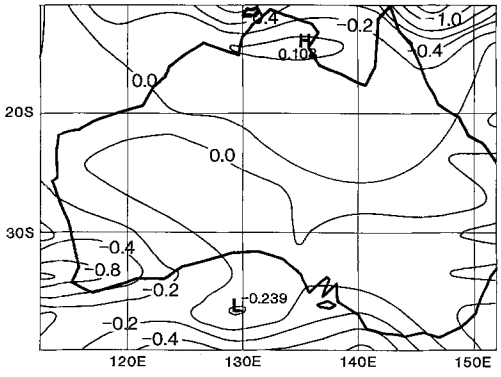

Fig. 14. As for Fig. 12a but for July conditions

occurring in the extreme southwest and southeast (Fig. 13b). Overnight minimum temperatures (Fig. 13c) fall by 1°–3° C over most of the country, with the greatest coolings in the north and the least in the southwest and southeast. Rainfall changes shown in Fig. 14 are generally small and irregular in space, indicating synoptic noise rather than a systematic reduction. This is reflected in an equally irregular pattern of changes in soil moisture (not shown).

Statistical significant of the results at individual grid points generally requires very long integrations due to the necessity of adequately sampling the synoptic variability. However, even with the present 100-day diurnal runs, the simulations enable us to examine the causal mechanism connecting these particular fluctuations in temperature, rainfall, soil moisture and solar irradiation at the surface; and these mechanisms may be expected to be of more general significance.

In Fig. 15 we see histograms of the 100 daily soil surface temperature maxima in the control and perturbed simulations, for a point in northeastern New South Wales (30° S, 152° E) for January conditions. Note that in both cases there appears to be a weak bimodal frequency distribution, with the warmer temperature (as we shall see below) corresponding to dry soil and the cooler to moist soil. With smoke overhead we see that both peaks occur at lower temperatures, with coolings being greatest in the case of dry soil. There is also a greater frequency of occurrence of temperatures corresponding to dry soil. In this case, although the temperature corresponding to dry soil dropped by several degrees, the median temperature in fact increased by 0.2° C, the average decreased by 1.1° C, and the upper quartile dropped by 2.6° C.

In contrast to the daily maximum temperatures, the overnight minima (shown in Fig. 16 for control and perturbed simulations) have a more monomodal frequency distribution and cool on average by only 0.3° C. The reason that the minimum temperature is not bimodally distributed is that the temperature at night is dominated by the long-wave radiation balance and not by latent heat and sensible heat fluxes as during the day. It is not, therefore, as greatly affected by soil moisture and is less affected by changes in the solar insolation than the daytime temperatures.

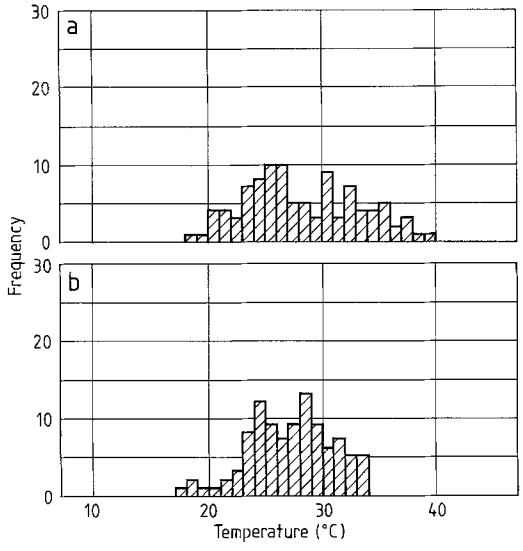

Fig. 15a, b. Frequency distributions of the 100 daily soil surface temperature maxima in **a** the control and **b** the perturbed simulations, for a grid point in northeastern New South Wales (30° S, 152° E) for January conditions

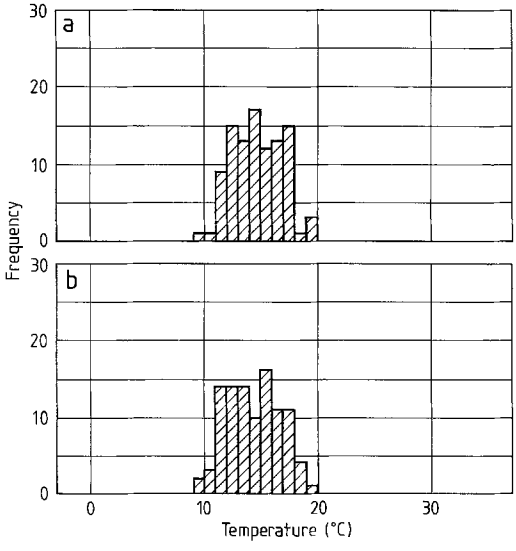

Fig. 16a, b. As for Fig. 15 but for daily minimum temperatures

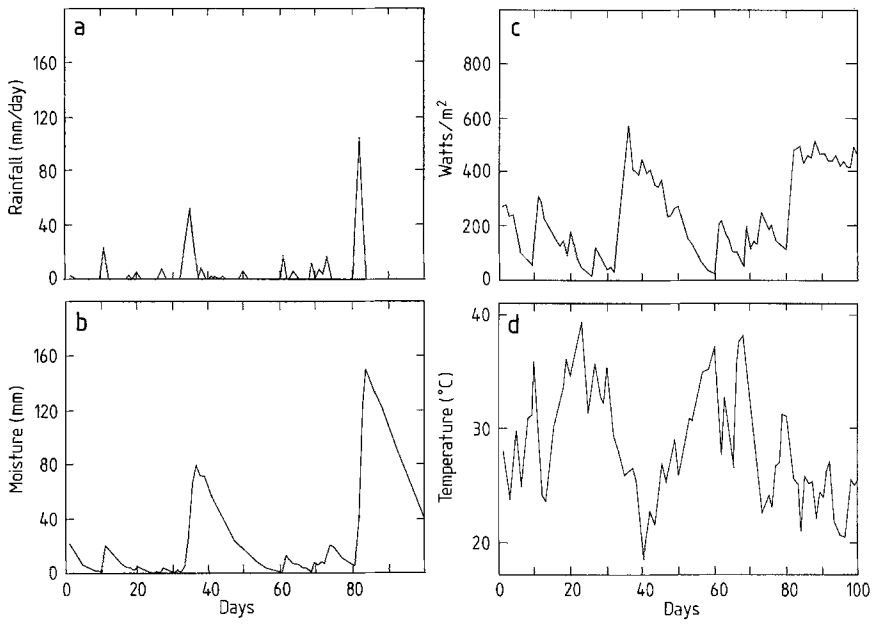

Fig. 17a, c. Time sequences over 100 days from the diurnal mode simulations for a grid point in northeastern New South Wales (30° S, 152° E) under January control conditions. Shown are **a** daily rainfall, **b** soil moisture, **c** mid-day evaporation and **d** daily maximum temperature

For the point in northeast New South Wales in January, the model gives a decrease in daily average rainfall rates from 3.7 mm/day in the control case to 2.1 mm/day in the perturbed case. This is sufficient to significantly change the soil moisture regime. The change at this grid point is consistent with the zonal mean rainfall changes shown in Fig. 7b, which is much more likely to be statistically significant since the zonal mean averages synoptic variations occurring over a large area. So, while the rainfall change at this one grid point may not be statistically significant per se, we believe it is qualitatively representative and that the causal connection with the surface temperature changes is illustrative of the physical interactions that could be important elsewhere.

Figure 17a shows a time sequence plot of daily rainfall at the above grid point for the 100 days of January control, while Fig. 17b shows the corresponding time sequence of soil moisture. The corresponding time sequences of mid-day evaporation and daily maximum temperatures are shown in Fig. 17c, d. Note the integrating effect of soil water capacity on rainfall, leading to relatively long spells of either almost dry or rather moist soil. This is reflected in relatively long spells of either high or low evaporation rates due to the highly non-linear relation between soil moisture and evaporation, with maximum temperatures showing a strong inverse correlation with evaporation. This accounts for the bimodal frequency distribution of maximum temperatures found in Fig. 15a. It should be noted, however, that this bimodal distribution could be, at least partly, an artifact of the limited vertical resolution of the soil model, which has an upper layer 5 cm thick. Nevertheless, we do not believe the result to be completely unrealistic, since observed daily surface maximum air temperatures from several Australian stations reveal similar bimodal frequency distributions during the wet season as shown by Hennessy and Pittock (personal communication).

Corresponding time sequence graphs are shown for the perturbed case in Fig. 18a–d for precipitation, soil moisture, evaporation and daily maximum temperature, respectively. Here we see a longer run of dry soil, relative to the control case, and that daily maximum temperatures in the case of dry soil are 2°–4° C lower than in the control.

In July at the same grid point, the model-generated rainfall rates in the control and perturbed simulations average 1.7 and 1.1 mm/day, respectively. The control rainfall is much less than in January, but is still sufficient to give appreciable periods of moist soil and a weakly bimodal distribution of daily maximum temperatures (Fig. 19a). The decrease in mean rainfall between the control and perturbed simulations now leads to no periods of near-saturated soil in the perturbed case, resulting in only a single peak in daily maximum temperatures (Fig. 19b). The cooling due to decreased solar insolation is reflected in a relatively large drop in surface temperature, averaging 3.8° C. As in January, daily minimum temperatures have a single peaked frequency distribution. In this case, the average cooling due to the smoke layer is 1.1° C (Fig. 20a, b).

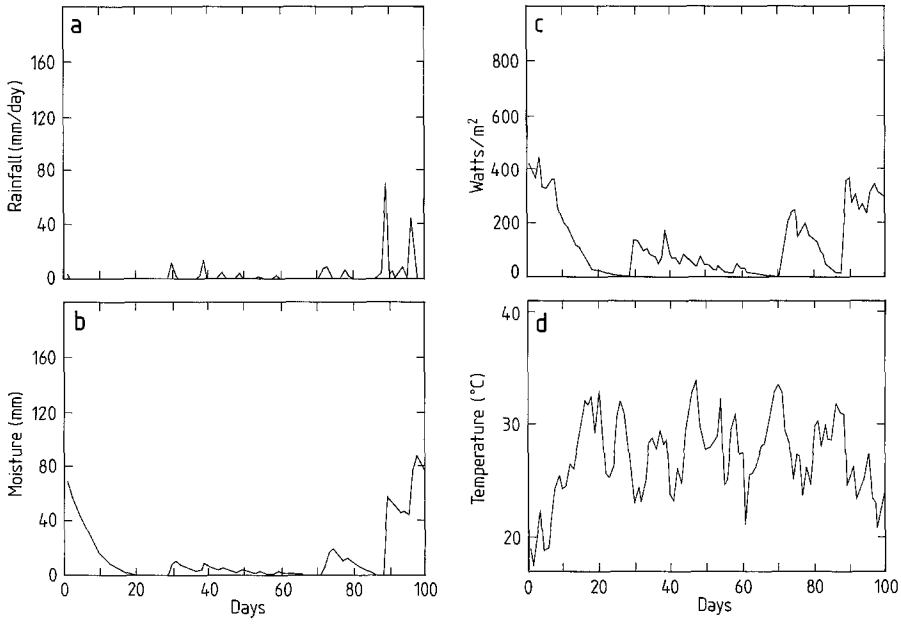

Fig. 18a, b. As for Fig. 17 but for the perturbed (smoke AOD = 0.2) simulation

At grid points with a more definite monsoonal rainfall distribution, the seasonal contrast in soil moisture regimes is more extreme. This leads, for instance at the grid point (11° S, 135° E) in northern Australia, to no change in the average daily maximum temperature between control and perturbed simulations in January, despite a marked change in the shape of the strongly bimodal frequency distribution which is reflected in a 2° C drop in the upper quartile temperature (Fig. 21a, b respectively). A cooling of 3.5° C is found in the dry season (Fig. 21c and d) in which the frequency distribution has only a single peak in both the control and perturbed simulations.

5 Discussion

5.1 Representativeness of the results

As already noted, one critical point is whether the present results provide us with a statistically significant and thus meaningful result. We have only integrated the control and perturbed runs for 105

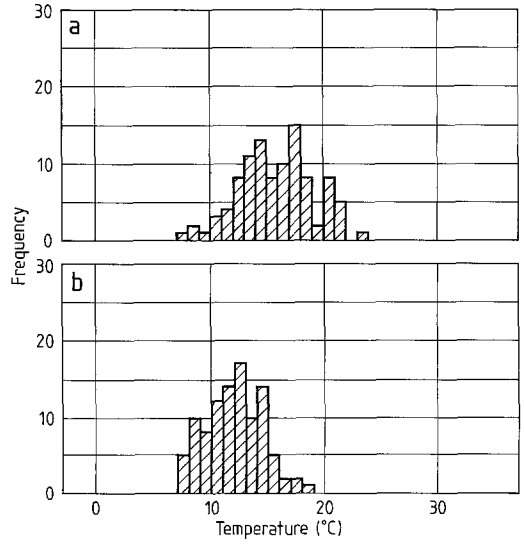

Fig. 19a, b. As for Fig. 15 but for July conditions

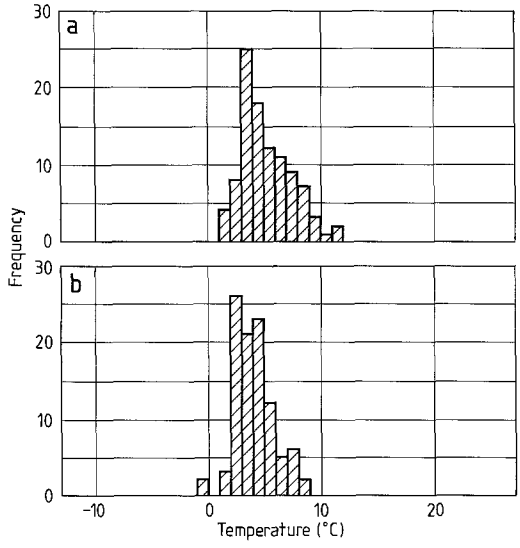

Fig. 20a, b. As for Fig. 15 but for daily minimum temperatures in July conditions

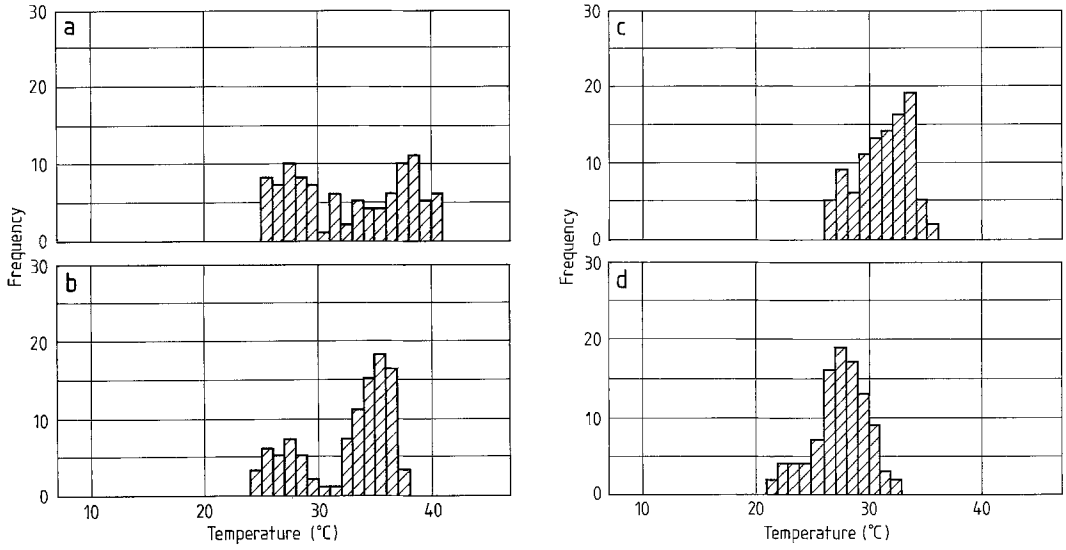

Fig. 21a–c. Frequency distributions of daily maximum temperatures at a grid point in northern Australia (11° S, 135° E) in **a** January control, **b** January perturbed, **c** July control and **d** July perturbed simulations

days without the diurnal cycle, and another 100 days with the diurnal cycle. At any one point on the globe, synoptic variability is such that a 100-day simulation is too short to capture a statistically representative sample of the possible synoptic variations which could occur there, which are dependent on the initial conditions. Yet it is prohibitively expensive to make multi-year integrations that might satisfy ideal statistical requirements. In any case, a similar problem would arise in reality since the detailed realisation of the perturbed climate, in the event of a nuclear war, would depend similarly on the initial conditions at the time of the war.

We therefore cannot claim with confidence that the geographical distribution of climatic anomalies found here, between the control and perturbed runs, is what would occur in reality. This is especially so, as the control model climate is far from perfect and, indeed, is quite poor for regional rainfall (see Hart et al. 1988). Nevertheless, we believe that the zonally averaged changes in temperature and precipitation are probably statistically significant and of the correct order of magnitude. This gains support from the consistency with time of the zonally averaged plots of temperature and rainfall, such as those shown in Figs. 1, 2 and 7. These average out spatially varying synoptic patterns and show no reversals of sign with time for the average differences.

Where we have presented frequency distributions and time series at a particular grid point, these should thus be taken as illustrative, and perhaps typical, of processes occurring at similar grid points rather than as quantitative descriptions of what might actually occur at that grid point in the real world. Such data help in understanding the processes leading to the zonal mean results, which probably have more quantitative meaning. We are further encouraged in this view by results obtained for temperature and the surface energy balance with a mesoscale model by Garratt, Pittock and Walsh (personal communication), as they are qualitatively and quantitatively consistent with the present results.

Another problem with the present simulations is the use of constant January or July conditions rather than a seasonal cycle. This might be expected — in areas where evaporation exceeds average precipitation — to lead to progressive drying of the soil over long runs, resulting in erroneously high surface temperatures. In the present simulations this does not appear to be a major problem — at least in the zonal mean land surface temperatures (Fig. 2), which show no significant rising trend over the 105 days of the diurnally averaged control run.

In our present model we also have fixed sea surface temperature and sea ice distribution. Both these factors in our model will reduce the "memory" of the climate system to the transient effects of the smoke, thus leading to an underestimation of the chronic stage effects (Robock 1984; Covey 1987).

The detailed results presented here are for the Australian region. However, the general conclusions which we draw are readily applicable to chronic conditions in the Northern Hemisphere 6

months to 1 year or more after a nuclear war, when the AOD of the smoke cloud would have fallen to approximately the levels assumed in this study. This is illustrated by the zonal mean results shown in Figs. 1 and 7, which indicate similar effects at northern latitudes for the same smoke AOD. The results may also be applicable to other aerosol forcings, such as a major volcanic eruption, although different assumptions would have to be made about the optical properties of a volcanic dust cloud in which scattering would be more important than absorption.

5.2 Rainfall reductions

Our results suggest that smoke amounts in the upper atmosphere of the order of AOD = 0.2 would cause major reductions in rainfall in the inter-tropical convergence zone and over land areas normally affected by monsoon rains. This might occur over the tropics and southern hemisphere in the first and possibly the second growing season after a major nuclear war in the northern spring or summer, and in the northern hemisphere in the second growing season.

Without any changes in sea surface temperature (as assumed in this simulation), no significant decrease in rainfall is found in the middle and high latitudes. This supports the view that a sudden decrease in solar insolation leads to a rapid suppression of convective activity, through large decreases in sensible and latent heat fluxes from the soil surface, but does not affect orographic or large-scale synoptic precipitation. The suggested decrease in convective activity is supported in detail by the studies of Garratt, Pittock and Walsh (personal communication) where a mesoscale model is used to study the surface energy balance: reduction of the solar insolation leads to a more stable atmospheric boundary layer.

When possible decreases in sea surface temperature due to reduced insolation are taken into account, further reductions in rainfall may be expected. Changes in sea surface temperature due to the presence of a smoke layer have been studied by Alexandrov and Stenchikov (1983), Robock (1984), Stenchikov (1985), Stenchikov and Carl (1985, 1987), Covey (1987), Mettlach et al. (1987) and Ghan et al. (1987). Walsh and Pittock (personal communication) find that for an elevated smoke layer having the properties assumed here, sea surface temperatures at 30° S would cool by about 2° C 6 months after a July war and by a similar amount 12 months after (due to a seasonal dependence in the cooling, which is generally a maximum in summer). If a smoke layer albedo of 0.2 is assumed as well, the cooling becomes nearer 4° C. Corresponding coolings at 45° S would be in the range 0.9°–3.4° C. Such coolings might be expected to lead to some reduction in rainfall in mid-latitudes as well as in the tropics and monsoon regions.

These results should be compared with those obtained by Ghan et al. (1988) in their GCM simulation in which interactive smoke is injected in target regions in the northern hemisphere and allowed to be lofted and transported by the modified atmospheric circulation. For total smoke injections in July of 50 million tonnes of smoke, they find that by days 20–30 after injection, precipitation rates in the inter-tropical convergence zone have decreased by some 20%, while those in middle latitudes of the northern hemisphere have decreased by 80% or more. Thus, a similar sensitivity is found in the tropics, but the suppression extends to higher latitudes. Rainfall suppression is not evident at this early stage in the southern hemisphere since appreciable smoke has not yet reached southern latitudes. The additional suppression of precipitation in mid northern latitudes is evidently due, in their case, to the presence of smoke in the upper troposphere, leading to a marked increase in vertical stability which confines mid-latitude synoptic activity to the lower troposphere. Indeed, the tropopause in simulations by Malone et al. (1986) is shown to reform at an altitude as low as 5 km. Such an effect is clearly not present in our simulation, where smoke is confined to the upper atmosphere above the top of the model, and would not be expected to occur in the southern hemisphere since most smoke at southern latitudes would be above 10 km according to the simulations of Malone et al. (1986) and others. Similar results to those of Ghan et al. (1988) are reported by Schneider and Thompson (1988) using the NCAR climate model.

5.3 Temperature changes

The model results show zonally averaged coolings of the land surface which average, in the daily mean, around 2°–4° C in both summer and winter and at all latitudes except those affected by the polar night. However, time series for individual grid points show days on which coolings in excess of 4° C occur, but others on which warmings occur at some locations. Examination of the daily temperature cycle shows, in general, that coolings are greater during the day than at night, relative to the control. Nevertheless, at some locations there

are days on which warmings of several degrees are found.

Areas of warming are found to correspond to areas where significant rainfall reductions occur, leading to dry soil and reductions in latent heat loss from the surface. Such warmings thus occur only in areas and seasons normally influenced by local or large-scale convective activity, notably areas of monsoon rainfall. Maximum coolings occur in relatively arid areas, the dry season, and in the higher latitudes where rainfall is not reduced.

Covey (1987) and Ghan et al. (1988) both found local warmings to occur at low latitudes, which they attributed to a combination of drier soil, increased downward infrared flux from the warm smoke layer, and other factors. In both of these simulations smoke was assumed to be present in the lower troposphere, which would enhance the surface warming effect at low AOD. This seems unrealistic for the chronic case, when one might expect tropospheric smoke to have been removed by washout processes. Moreover, the additional downwards infrared flux from the smoke must be less than the loss of solar insolation at the surface due to absorption in the visible, so additional downwards infrared by itself cannot account for surface warming.

Our results highlight the importance of changes in soil moisture under conditions of climatic change, not only for its direct agricultural consequences but also for its effect on surface temperature. It is also noteworthy that daily maximum temperatures are more sensitive to changes in solar insolation than is the overnight minimum. This means that calculated changes in the daily mean temperature cannot be simply translated into changes in daily minima and thus to changes in frost frequency.

It should be noted that the amplitudes of the daily soil surface temperature cycle in the control simulations are smaller than observed. This is probably due to the crude soil model in which the top layer is 5 cm thick. The relatively large heat capacity of this layer tends to smooth out the diurnal temperature cycle at the surface proper.

Assumptions and simplifications in the present simulation may affect the temperature results. These include neglect of downward infrared radiation emitted by the warm layer of smoke, constant climatological mean cloud cover, neglect of smoke cloud albedo, assumed constant climatological sea surface temperatures and fixed sea ice distribution.

As discussed earlier, we believe that neglect of the downward IR from the smoke will restore only a fraction (of the order of one-sixth) of the energy lost to the surface due to smoke absorption in the visible. This neglect thus leads to only a slight overestimation of the daytime cooling, but to a rather larger overestimation of the night-time cooling (when solar insolation is absent, but smoke IR is present).

As the model predicts changes in rainfall, and these will in general correspond to changes in cloud cover (which is held fixed in calculating the radiative balance of the atmosphere), variable cloud cover might be expected to reinforce the tendency for daytime warming in areas where rainfall is suppressed. As we have already seen, the effect of reduction in soil moisture is already significant in such areas. Reductions in cloud cover will tend to allow more infrared heat loss from the surface at night, and thus lead to lower overnight minima in these areas of daytime warming. Areas that in reality are cloud-free, but which in the model have the same non-zero cloud cover in control and perturbed cases, would be expected in reality to exhibit a somewhat larger cooling due to presence of smoke absorption, compared with the model results. Those areas where cloudiness is due to large-scale synoptic systems are not expected to be affected by the neglect of variable cloudiness, provided sea surface temperature remains constant.

Neglect of smoke cloud albedo will, in general, lead to an underestimation of the surface cooling. In the case of sea surface temperature, Walsh and Pittock (personal communication) have shown that this neglect may lead to significant underestimation of surface cooling. However, they have not evaluated the effect over land.

Prescribed sea surface temperatures in the present simulations will lead to an underestimation of cooling over land, particularly in coastal areas with onshore winds. Lower sea surface temperatures in middle latitudes could lead to reductions in cloud cover, less rainfall, drier soil, reduced tropospheric water vapour content, and less reduction in solar insolation during the day but greater heat losses at night. Thus, daytime coolings could be reduced but night-time coolings might be increased, with lower dew points and a greater incidence of frosts.

5.4 Other biologically significant changes

Several other changes in climatic conditions of biological importance might be expected to occur in the southern hemisphere due to the presence of smoke in the upper atmosphere following a major

nuclear war. These include a reduction in the effective length of daylight and in available sunlight for photosynthesis, and a possible large increase in the intensity of biologically active ultraviolet radiation (UV-B) (Vupputuri 1986). Recent results suggest as much as a 50% decrease in global ozone within a few months after a nuclear war (Schneider 1988), which may significantly increase the intensity of UV-B radiation reaching the surface even in the presence of a thin layer of smoke. We have not extended calculations of these effects beyond those reported in the SCOPE study (Pittock et al. 1986; Pittock 1987) and in Turco and Golitsyn (1988).

6 Conclusions

Numerous studies (Pittock et al. 1986; Malone et al. 1986, and others) lead to the conclusion that, in the event of a major nuclear war in the northern hemisphere, a layer of smoke of absorption optical thickness around 0.2 might well spread over Australia at high altitudes within a matter of weeks and remain over Australia for up to 12 months or more (Stephens et al. 1988).

Taking that as our starting point, we have used three main approaches to estimating the possible climatic effects over Australia. This paper, in particular, reports on the use of a three-dimensional climate model simulation of the effect of a uniform elevated smoke layer. Various simplifying assumptions — notably, neglect of infrared absorption and visible scattering by the smoke, and fixed cloud cover and sea surface temperature — were made. The possible effects of these assumptions have been discussed.

We conclude that the principal climatic effects of the smoke would be to reduce convective rainfall over Australia by the order of 50%, and to reduce soil surface temperatures by several degrees C except in those locations and seasons where reduction in soil moisture is sufficient to effectively stop evaporation from the soil surface. In that case, small increases in temperature may occur.

Daily maximum temperatures are more strongly affected, with coolings of the order of 2° or 3° C in summer (with some local warmings) and 4°–6° C in winter, if we neglect the progressive cooling of the ocean surface. Overnight minimum temperatures would cool by 1° or 2° C in both summer and winter. Cooling of the ocean surface might add to the land surface effect (particularly in coastal areas), as would inclusion of scattering of sunlight by the smoke. On the other hand, infrared absorption and emission by the smoke would tend to decrease the overnight minimum coolings but have little effect on the daily maxima. Rainfall decrease might be enhanced, especially at higher latitudes, by cooling of the ocean surface.

On the basis of these climatic results, and taking account of various other biologically significant stresses, we have evaluated the possible effect on primary production in Australia in a study to be reported elsewhere.

The implications of this work for estimates of the climatic effects and their consequences outside Australia are perhaps more severe than for Australia itself. The climate modelling suggests that a substantial failure of monsoon rains may be expected in the tropics for smoke amounts which seem highly probable in the first growing season, and possibly in the second growing season, after a nuclear war. This raises the spectre of large and prolonged food shortages in many highly populated areas of the world, leading to widespread starvation, as foreshadowed by Harwell and Hutchinson (1985). The present results add credibility to those calculations and conclusions, viz. that more people may die from mass starvation in the developing countries as a result of nuclear war than would die from the direct effects in the combatant countries.

More precise estimates of the consequences of a possible nuclear war (either for Australia or elsewhere) clearly require further research, for example using a model with a fully interactive ocean, inclusion of smoke albedo and infrared absorption properties, better representation of soil heat capacity and hydrology, and better representation of climate-vegetation interactions. In view of the basic uncertainties in the nuclear war scenario itself, and the chance occurrence of a particular realisation of climate variability at the time of the war, it is doubtful how far one should go down this road for studies of the effects of nuclear war. Perhaps the lesson is already clear enough.

On the other hand, there are close parallels between attempts to simulate the climatic effects of nuclear war and attempts to model the climatic consequences of the greenhouse effect, which physically is almost the exact converse of the "nuclear winter" problem (Turco et al. 1983; Pittock 1988). Thus, most of the model improvements mentioned in the preceding paragraph are required to better predict the regional consequences of the greenhouse warming. Indeed, we may already learn from the nuclear war effect simulations, for example that convective rainfall is parti-

cularly sensitive to changes in the surface radiation balance and that changes in daily mean temperatures may result from quite different effects on the overnight minima and daily maxima. Moreover, the importance of the soil moisture regime has been highlighted. These are important lessons for future work on the greenhouse effect.

Acknowledgements. This work was made possible by a grant from the Australian Government through the Department of Foreign Affairs, and was largely inspired by the international research effort on the environmental effects of nuclear war which was coordinated by the Scientific Committee on Problems of the Environment under the leadership of Sir Frederick Warner. Useful encouragement and advice was received from R.C. Malone of the Los Alamos National Laboratory, New Mexico. The authors are particularly indebted to the scientists who built the climate model at the former Australian Numerical Meteorology Research Centre and the present Bureau of Meteorology Research Centre, notably W.P. Bourke, T.L. Hart, B.J. McAvaney, J.L. McGregor, and K. Puri. In particular, B.J. McAvaney was responsible for the recent vectorization of the model for use on the Cyber 205 computer.

References

Alexandrov V, Stenchikov GL (1983) On the modelling of the climate consequences of nuclear war. Proc Appl Maths, Computing Centre USSR Academy of Sciences, Moscow, pp 21

Berry MV, Percival IC (1986) Optics of fractal clusters such as smoke. Optica Acta 33:577–591

Clarke RH, Brook RR (eds) (1979) The Koorin expedition — Atmospheric boundary layer data over tropical savannah land. Dept of Science and Environment. Austr Govt Printing Service, Canberra, pp 359

Covey C (1987) Protracted climatic effects of massive smoke injections into the atmosphere. Nature 325:701–703

Crutzen PJ, Birks JW (1982) The atmosphere after a nuclear war. Ambio 11:114–125

de Haas N, Fristrom RM, Linevsky MJ, Silver DM (1986) Smoke scavenging by atmospheric ozone as a possible factor in the nuclear winter problem. Johns Hopkins APL Tech Digest 7:181–186

Ghan SJ, MacCracken MC, Walton JJ (1987) Chronic effects of large atmospheric smoke injections: interactions with the ocean mixed layer, sea ice and ground hydrology. Tech Papers, DNA Global Effects Program Review 7-9 April 1987, DASIAC-TN-87-35-V3, Defense Nuclear Agency, Washington D.C.

Ghan SJ, MacCracken MC, Walton JJ (1988) The climatic response to large atmospheric smoke injections: sensitivity studies with a tropospheric general circulation model. J Geophys Res 93:8315–8338

Hart TL, Bourke WP, McAvaney BJ, Forgan BW, McGregor JL (1988) Atmospheric general circulation simulation with the BMRC global spectral model: the impact of revised physical parameterizations. Bur Meteorol Res Centre Res Rep No 12

Harwell M, Hutchinson TC (1985) Environmental consequences of nuclear war: Vol II. Ecological and agricultural effects. SCOPE 28. Wiley, Chichester, pp 554

Malone RC, Auer LH, Glatzmaier GA, Wood M (1986) Nuclear winter: three-dimensional simulations including interactive transport, scavenging, and solar heating of smoke. J Geophys Res 91:1039–1053

McAvaney BJ, Bourke W, Puri K (1978) A global spectral model for simulation of the general circulation. J Atmos Sci 35:1557–1583

Mettlach TR, Haney RL, Garwood RW Jr, Ghan SJ (1987) The response of the upper ocean to a large summertime injection of smoke into the atmosphere. J Geophys Res 92:1969–1979

Mitchell JFB, Slingo A (1988) Climatic effects of nuclear war. J Geophys Res 93:1031–1045

NAS (1985) The effects on the atmosphere of a major nuclear exchange. National Academy Press, Washington, pp 193

Penner JE (1986) Uncertainties in the smoke source term for 'nuclear winter' studies. Nature 324:222–226

Pittock AB (1986) Rapid developments on nuclear winter. Search 17:23–24

Pittock AB (1987) Beyond darkness: nuclear winter in Australia and New Zealand. Sun Books, South Melbourne, pp 264

Pittock AB (1988) Climatic catastrophes: the local and global effects of greenhouse gases and nuclear winter. In El-Sabh MI, Murphy TS (eds), Natural and Man-Made Hazards. Reidel, Dordrecht, 621–633 pp

Pittock AB, Ackerman TP, Crutzen PJ, MacCracken MC, Shapiro CS, Turco RP (1986) Environmental consequences of nuclear war: Vol I. Physical and atmospheric effects. SCOPE 28, Wiley, Chichester, pp 374

Pittock AB, Frederiksen JS, Garratt JR, Walsh K (1989) Climatic effects of smoke and dust produced from nuclear conflagrations. In: Hobbs PV, McCormick MP (eds) Aerosols and climate. Deepak Pub, Hampton, 395–410 pp

Post MJ (1986) Atmospheric purging of El Chichon debris. J Geophys Res 91:5222–5228

Ramaswamy V, Kiehl JT (1985) Sensitivities of the radiative forcing due to large loadings of smoke and dust aerosols. J Geophys Res 90:5597–5613

Robock A (1984) Snow and ice feedbacks for prolonged effects of nuclear winter. Nature 310:667–670

Schneider SH (1988) Whatever happened to nuclear winter? — An editorial. Climatic Change 12:215–219

Schneider SH, Thompson SL (1988) Simulating the climatic effects of nuclear war. Nature 333:221–227

Stenchikov GL (1985) Mathematical modelling of the influence of the atmospheric pollution on climate and nature. Proc Appl Math, Computing Centre of the USSR Academy of Sciences, Moscow, pp 19

Stenchikov GL, Carl P (1985) Sensitivity against large-scale inhomogeneities in the initial atmospheric pollutions. Paper presented at conference on "Climatic Consequences of Nuclear War", Berlin (GDR), October 1985, pp 56

Stenchikov GL, Carl P (1987) The complex nature of climate systems after nuclear war. Paper presented at SCOPE-ENUWAR workshop, Bangkok, February 1987

Stephens SL, Calvert JG, Birks JW (1988) Ozone as a sink for atmospheric carbon aerosols: today and following a nuclear war. Aerosol Sci Tech (in press)

Turco RP, Golitsyn GS (1988) Global effects of nuclear war. Environment 30:8–16

Turco RP, Toon OB, Ackerman TP, Pollack JB, Sagan C (1983) Nuclear winter: global consequences of multiple nuclear explosions. Science 222:1283–1292

Vupputuri RKR (1986) The effect of ozone photochemistry on atmospheric and surface changes due to large injections of smoke and NO_x by a large-scale nuclear war. Atmos Environ 20:665–680

Warner F, and collaborators (1987) Severe global-scale effects of nuclear war reaffirmed. Environment 29:4–5 & 45

Received August 22, 1988/Accepted November 11, 1988